

# Measurement of the differential cross sections of the $\Sigma^-p$ elastic scattering in momentum range 470 to 850 MeV/c

K. Miwa<sup>1</sup>, J.K. Ahn<sup>2</sup>, Y. Akazawa<sup>3</sup>, T. Aramaki<sup>1</sup>, S. Ashikaga<sup>4</sup>, S. Callier<sup>5</sup>, N. Chiga<sup>1</sup>, S. W. Choi<sup>2</sup>, H. Ekawa<sup>6</sup>, P. Evtoukhovitch<sup>7</sup>, N. Fujioka<sup>1</sup>, M. Fujita<sup>8</sup>, T. Gogami<sup>4</sup>, T. Harada<sup>4</sup>, S. Hasegawa<sup>8</sup>, S. H. Hayakawa<sup>1</sup>, R. Honda<sup>3</sup>, S. Hoshino<sup>9</sup>, K. Hosomi<sup>8</sup>, M. Ichikawa<sup>4,14</sup>, Y. Ichikawa<sup>8</sup>, M. Ieiri<sup>3</sup>, M. Ikeda<sup>1</sup>, K. Imai<sup>8</sup>, Y. Ishikawa<sup>1</sup>, S. Ishimoto<sup>3</sup>, W. S. Jung<sup>2</sup>, S. Kajikawa<sup>1</sup>, H. Kanauchi<sup>1</sup>, H. Kanda<sup>10</sup>, T. Kitaoka<sup>1</sup>, B. M. Kang<sup>2</sup>, H. Kawai<sup>11</sup>, S. H. Kim<sup>2</sup>, K. Kobayashi<sup>9</sup>, T. Koike<sup>1</sup>, K. Matsuda<sup>1</sup>, Y. Matsumoto<sup>1</sup>, S. Nagao<sup>1</sup>, R. Nagatomi<sup>9</sup>, Y. Nakada<sup>9</sup>, M. Nakagawa<sup>6</sup>, I. Nakamura<sup>3</sup>, T. Nanamura<sup>4,8</sup>, M. Naruki<sup>4</sup>, S. Ozawa<sup>1</sup>, L. Raux<sup>5</sup>, T. G. Rogers<sup>1</sup>, A. Sakaguchi<sup>9</sup>, T. Sakao<sup>1</sup>, H. Sako<sup>8</sup>, S. Sato<sup>8</sup>, T. Shiozaki<sup>1</sup>, K. Shirotori<sup>10</sup>, K. N. Suzuki<sup>4</sup>, S. Suzuki<sup>3</sup>, M. Tabata<sup>11</sup>, C. d. L. Taille<sup>5</sup>, H. Takahashi<sup>3</sup>, T. Takahashi<sup>3</sup>, T. N. Takahashi<sup>10</sup>, H. Tamura<sup>1,8</sup>, M. Tanaka<sup>3</sup>, K. Tanida<sup>8</sup>, Z. Tsamalaidze<sup>7,12</sup>, M. Ukai<sup>3</sup>, H. Umetsu<sup>1</sup>, S. Wada<sup>1</sup>, T. O. Yamamoto<sup>8</sup>, J. Yoshida<sup>1</sup>, K. Yoshimura<sup>13</sup>

<sup>1</sup> Department of Physics, Tohoku University, Sendai 980-8578, Japan.

<sup>2</sup> Department of Physics, Korea University, Seoul 02841, Korea

<sup>3</sup> Institute of Particle and Nuclear Studies (IPNS),

High Energy Accelerator Research Organization (KEK), Tsukuba 305-0801, Japan

<sup>4</sup> Department of Physics, Kyoto University, Kyoto 606-8502, Japan

<sup>5</sup> OMEGA Ecole Polytechnique-CNRS/IN2P3, 3 rue Michel-Ange, 75794 Paris 16, France

<sup>6</sup> High Energy Nuclear Physics Laboratory, RIKEN, Wako, 351-0198, Japan

<sup>7</sup> Joint Institute for Nuclear Research (JINR), Dubna, Moscow Region 141980, Russia

<sup>8</sup> Advanced Science Research Center (ASRC), Japan Atomic Energy Agency (JAEA), Tokai, Ibaraki 319-1195, Japan

<sup>9</sup> Department of Physics, Osaka University, Toyonaka 560-0043, Japan

<sup>10</sup> Research Center for Nuclear Physics (RCNP), Osaka University, Ibaraki 567-0047, Japan

<sup>11</sup> Department of Physics, Chiba University, Chiba 263-8522, Japan

<sup>12</sup> Georgian Technical University (GTU), Tbilisi, Georgia

<sup>13</sup> Department of Physics, Okayama University, Okayama 700-8530, Japan and

<sup>14</sup> Meson Science Laboratory, Cluster for Pioneering Research, RIKEN, Wako, 351-0198, Japan

(J-PARC E40 Collaboration)

(Dated: April 29, 2021)

A high statistics  $\Sigma p$  scattering experiment has been performed at the J-PARC Hadron Experimental Facility. Data for momentum-tagged  $\Sigma^-$  running in a liquid hydrogen target were accumulated by detecting the  $\pi^- p \rightarrow K^+ \Sigma^-$  reaction with a high intensity  $\pi^-$  beam of 20 M/spill. Differential cross sections of the  $\Sigma^- p$  elastic scattering were derived with a drastically improved accuracy by identifying the largest statistics of about 4,500 events from  $1.72 \times 10^7 \Sigma^-$ . The derived differential cross section shows a clear forward-peaking angular distribution for a  $\Sigma^-$  momentum range from 470 to 850 MeV/c. The accurate data will impose a strong constraint on the theoretical models of the baryon-baryon interactions.

The interactions between octet baryons, that is, baryon-baryon ( $BB$ ) interactions including hyperon-nucleon ( $YN$ ) and hyperon-hyperon ( $YY$ ) interactions have been intensively studied both theoretically and experimentally. The Nijmegen group [1, 2] and the Jülich group [3] have constructed their own  $BB$  interaction models with a unified description based on the boson-exchange picture assuming the flavor SU(3) symmetry. The role of quarks in the  $BB$  interactions was studied by the Quark Cluster Model (QCM) by taking into account the effect of the Pauli principle for quarks and the color magnetic interaction [4]. QCM predicts characteristic nature in the short-range region such as a strongly repulsive core or an attractive interaction depending on the spin and flavor configuration of the quarks in the system. The realistic description based on the quark picture has been constructed by incorporating an effective meson exchange potential in QCM to represent the middle and long range interactions by the Kyoto-Niigata group [5]. These pre-

dictions are now reproduced by lattice QCD simulations which become a powerful theoretical tool to drive the  $YN$  and  $YY$  potentials from the first principle in QCD [6–8]. A modern description based on the chiral effective field theory ( $\chi$ EFT) has been extended to the  $YN$  sector up to the next leading order [9, 10]. In order to test and improve these theoretical models of the  $BB$  interactions, important experimental inputs must be two-body scattering data between a hyperon and a proton. In the case of the  $NN$  interaction (nuclear force), the  $pp$  and  $np$  scattering data played essential roles to establish the realistic nuclear force models [11–13]. On the other hand, no experimental progress in hyperon-proton scattering has been made since 1970s due to experimental difficulties stemming from low intensity of the hyperon and its short lifetime [14–22]. Therefore, historically, the  $BB$  interactions have been investigated from hypernuclear data because their binding energies and energy levels reflect the  $YN$  interactions [23, 24]. Since observation of a mas-

sive neutron star with two-solar mass [25], existence of a three-body repulsive interaction including hyperons has been discussed as a possible source of supporting such massive stars [26]. In order to derive properties of such  $YN$  three-body interaction from hypernuclear structure, the  $YN$  two-body interaction should be determined from the two-body system to eliminate uncertainties from many-body effects in the hypernuclear system. In such situation, construction of a realistic two-body  $YN$  interaction via high statistics hyperon-proton scattering data is crucially important.

As a first step to realize such accurate hyperon-proton scattering experiments, a new  $\Sigma p$  scattering experiment was performed in J-PARC to provide accurate differential cross sections of the  $\Sigma^+p$ ,  $\Sigma^-p$  elastic scatterings and the  $\Sigma^-p \rightarrow \Lambda n$  inelastic scattering. Theoretically the  $\Sigma N$  interaction is predicted to be strongly spin-isospin dependent. The only observed  $\Sigma$  hypernucleus ( ${}^4_\Sigma\text{He}$ ) [27] is bound by the attractive interaction in the ( $I = 1/2$ ,  $S = 1$ ) channel. On the other hand, the spin and isospin averaged  $\Sigma$ -nucleus potential was confirmed to be strongly repulsive from  $\Sigma$  quasi-free production spectra in several nuclei [28, 29]. In order to investigate the  $\Sigma N$  interaction for each spin-isospin channel more quantitatively, systematic measurement of these three scattering channels is important. In this letter, we present the differential cross section of the  $\Sigma^-p$  elastic scattering in the  $\Sigma^-$  momentum region ranging from 470 to 850 MeV/c as the first result of this systematic measurement. The existing differential cross sections of the  $\Sigma^-p$  scattering are limited to the  $S$ -wave dominant region of a beam momentum around 300 MeV/c [18–20] except for a few higher momentum data with insufficient accuracy [21]. Therefore, there are no data to determine the  $P$ - and higher partial waves of the  $\Sigma p$  channel [9, 10]. Especially, in the  $\Sigma^-p$  channel, all theoretical models predict a large angular dependence in the differential cross section in the  $\Sigma^-$  momentum range higher than 500 MeV/c due to the higher partial wave contribution. Precise measurement of the differential cross section of the  $\Sigma^-p$  elastic scattering in this momentum region is indispensable to impose a strong constraint on the theoretical models.

The  $\Sigma p$  scattering experiment (J-PARC E40) [30, 31] was performed at the K1.8 beam line in the J-PARC Hadron Experimental Facility. A 1.33 GeV/c  $\pi^-$  beam of  $2.0 \times 10^7$ /spill was produced from 30 GeV proton beam with a spill cycle of 5.2 seconds with a beam duration of 2 seconds. FIG. 1 shows the experimental concept and the experimental setup around a liquid hydrogen (LH<sub>2</sub>) target.  $\Sigma^-$  particles are produced by the  $\pi^-p \rightarrow K^+\Sigma^-$  reaction and the produced  $\Sigma^-$  running in the LH<sub>2</sub> target interacts with protons with a certain probability. The momentum of each  $\Sigma^-$  can be tagged as the missing momentum calculated from the momenta of  $\pi^-$  beam and outgoing  $K^+$  analyzed by the K1.8 beam line spectrometer [32] and the forward magnetic (KURAMA) spectrom-

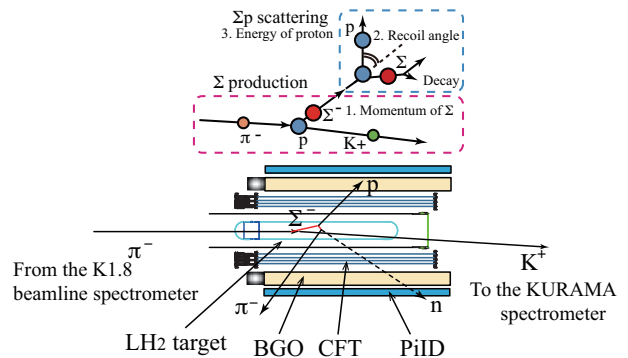


FIG. 1. Experimental concept of the  $\Sigma p$  scattering experiment and the experimental setup around the LH<sub>2</sub> target. Two successive two-body reactions of the  $\Sigma^-$  production ( $\pi^-p \rightarrow K^+\Sigma^-$ ) and the  $\Sigma^-p$  scattering ( $\Sigma^-p \rightarrow \Sigma^-p$ ) are detected. The  $\Sigma p$  scattering events are detected by the CATCH system which surrounds the LH<sub>2</sub> target.

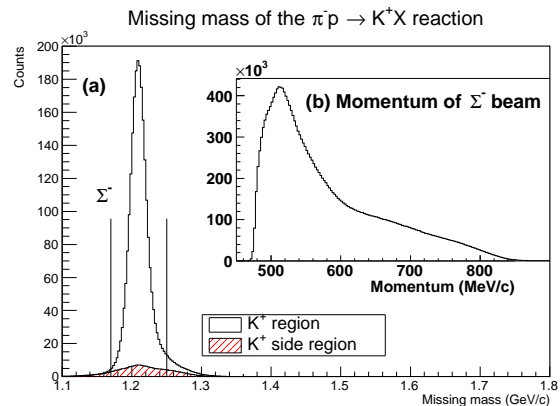


FIG. 2. (a) Missing mass spectra of the  $\pi^-p \rightarrow K^+X$  reaction for  $K^+$  events (open histogram) and side-band events of  $K^+$  (filled histogram) to estimate the effect of the contamination of the miscalculated event under the  $K^+$  region in mass square spectrum. Two lines show the selected area for the  $\Sigma^-$  particles. (b)  $\Sigma^-$  momentum reconstructed as the missing momentum of the  $\pi^-p \rightarrow K^+\Sigma^-$  reaction.

eter, respectively. A recoil proton knocked out by the  $\Sigma^-p$  scattering is detected by the CATCH system, which consisted of a cylindrical scintillation fiber tracker (CFT), a BGO calorimeter (BGO) and a scintillator hodoscope (PiID) coaxially arranged from inner to outer sides [33]. The  $\Sigma^-p$  elastic scattering can be identified by checking the kinematical consistency between the scattering angle and the kinetic energy of the recoil proton measured by CFT and BGO, respectively.

$\Sigma^-$  is identified by the missing mass spectrum of the  $\pi^-p \rightarrow K^+X$  reaction as shown in FIG. 2 (a). A clear peak corresponding to  $\Sigma^-$  is identified. The histogram filled by slashed lines shows contribution from the contamination of  $\pi^+$  and proton in the  $K^+$  selection due

to miscalculation of the time-of-flight caused by multiple beam events. The contamination was estimated from the side-band events of the  $K^+$  mass region by scaling to the number of contaminating events in the  $K^+$  mass gate. We selected the missing mass region from 1.17 to 1.25  $\text{GeV}/c^2$  as  $\Sigma^-$  and the contamination fraction was estimated to be 7.5%. In total, the  $\Sigma^-$  particles of  $1.62 \times 10^7$ , that is, typically 100 times larger number than that in a past experiment [21], were accumulated after subtracting the contamination. The reconstructed  $\Sigma^-$  momentum ranged from 470 to 850  $\text{MeV}/c$  continuously as shown in FIG. 2 (b).

For the analysis of the  $\Sigma^-p$  scattering, a proton was searched for with CATCH in coincidence with the  $\Sigma^-$  production. The particle identification between  $\pi$  and proton was performed by the  $dE$ - $E$  method between the partial energy deposit ( $dE$ ) in CFT and the total energy deposit ( $E$ ) in BGO. For  $\pi$ , the thickness of BGO was not sufficient to stop  $\pi$ 's and only the direction was obtained by the CFT tracking. The momentum estimation of  $\pi$  is described later. For the proton, its kinetic energy and direction could be measured by CATCH. Because  $\Sigma^-$  has no decay channel to a proton, the detected proton is a sign of the secondary  $\Sigma^-p$  reactions including the  $\Sigma^-p$  elastic scattering and the  $\Sigma^-p \rightarrow \Lambda n, \Sigma^0 n$  inelastic scatterings. However, many of these protons were originated from the secondary  $np$  and  $\pi^-p$  reactions after the  $\Sigma^- \rightarrow n\pi^-$  decay.

Then, we explain how the scattering events can be identified by taking an example of the  $\Sigma^-p$  elastic scattering. The momentum vector of the  $\Sigma^-$  particle is reconstructed from the spectrometer information. The recoil angle of proton can be obtained as the crossing angle between the  $\Sigma^-$  and the proton tracks. The proton's energy can be calculated from the recoil angle of the proton by applying the  $\Sigma^-p$  elastic scattering kinematics. Here, the calculated energy is described as  $E_{\text{calculated}}$ . On the other hand, the proton energy was measured by BGO and the measured energy is denoted as  $E_{\text{measured}}$  here. Then we define  $\Delta E(\Sigma^-p)$  as the difference between  $E_{\text{measured}}$  and  $E_{\text{calculated}}$ , that is,  $\Delta E(\Sigma^-p) = E_{\text{measured}} - E_{\text{calculated}}$ , under the  $\Sigma^-p$  elastic scattering assumption. If the recoil proton really originated in the  $\Sigma^-p$  elastic scattering, such events would make a peak around  $\Delta E(\Sigma^-p) = 0$  in the  $\Delta E(\Sigma^-p)$  spectrum. We checked the kinematical consistencies for all possible secondary reactions, that is,  $np, \pi^-p, \Sigma^-p$  elastic scatterings and  $\Sigma^-p \rightarrow \Lambda n$  reaction in the same manner as described in the  $\Sigma^-p$  scattering case except for the  $\Sigma^-p \rightarrow \Sigma^0 n$  reaction where kinematical reconstruction was impossible due to the missing information of  $\gamma$  from the  $\Sigma^0$  decay. In these calculations, the  $\pi^-$  momentum was determined by imposing some assumptions corresponding to each reaction. In the  $np$  scattering, a similar value of  $\Delta E(np)$  was defined as the difference between  $E_{\text{measure}}$  and  $E_{\text{calculated}}$  calculated from the recoil

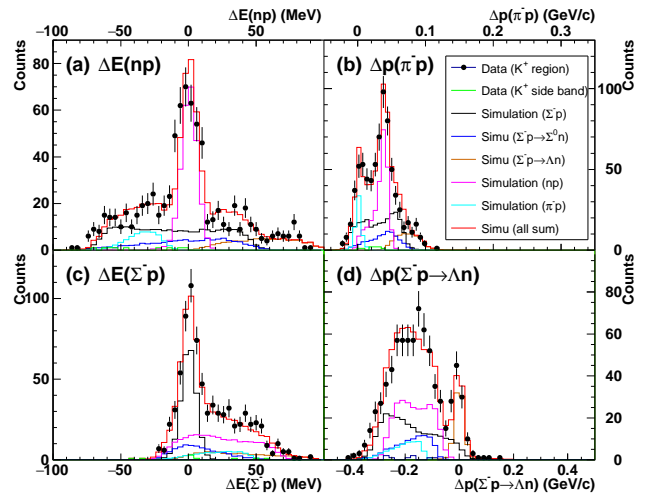


FIG. 3. Kinematical consistency between the measured energy and the calculated energy from the measured scattering angle assuming the four different scattering processes, (a)  $\Delta E(np)$ , (b)  $\Delta p(\pi^-p)$ , (c)  $\Delta E(\Sigma^-p)$ , and (d)  $\Delta p(\Sigma^-p \rightarrow \Lambda n)$  distributions, for the angular region of  $0 \leq \cos \theta \leq 0.1$  in the momentum range of  $470 < p \text{ (MeV}/c) < 550$ . Data points with error bars and histograms with a green line show the experimental data for the  $K^+$  region and the side-band region of  $K^+$  in the mass square spectrum, respectively. Simulated spectra for assumed reactions were also shown and the histogram of a red line shows the sum of these spectra.

angle based on the  $np$  scattering kinematics, where the initial neutron momentum was determined by assuming  $\pi^-$  was emitted in the  $\Sigma^-$  decay. Similarly, in case of the  $\Sigma^-p \rightarrow \Lambda n$  reaction assumption,  $\Delta p(\Sigma^-p \rightarrow \Lambda n)$  was defined as the difference between  $\Lambda$  momentum calculated from the scattering angle and that reconstructed from the  $\Lambda$  decay where the momentum magnitude of  $\pi^-$  was determined so that the invariant mass of  $\pi^-$  and proton became the  $\Lambda$  mass. In the  $\pi^-p$  scattering, similar momentum difference  $\Delta p(\pi^-p)$  was obtained for recoil proton. FIG. 3 shows the four kinematical plots for (a)  $np$ , (b)  $\pi^-p$ , (c)  $\Sigma^-p$  and (d)  $\Sigma^-p \rightarrow \Lambda n$  reactions for a scattering angular region of  $0 \leq \cos \theta \leq 0.1$  in the momentum range of  $470 < p \text{ (MeV}/c) < 550$ . The contribution from each reaction can be well estimated by fitting the four kinematical spectra simultaneously with the simulated spectra for each reaction as shown in colored histograms in FIG. 3. For example, the  $np$  scattering events forms the peak structure in FIG. 3 (a)  $\Delta E(np)$ , whereas it makes the background structure for other spectra. Here, we also took into account the misidentification event of  $K^+$  by selecting the side-band events of  $K^+$  in the mass square spectrum, although the contribution was negligibly small. The peaks in FIG. 3 (c) and (d) correspond to the  $\Sigma^-p$  elastic scattering and the  $\Sigma^-p \rightarrow \Lambda n$  scatter-

ing. In order to improve the S/N ratio in the  $\Delta E(\Sigma^-p)$  spectrum, events around the peak regions of the  $\Delta E(np)$ ,  $\Delta p(\pi^-p)$  and  $\Delta p(\Sigma^-p \rightarrow \Lambda n)$  spectra were removed. Finally, about 4,500 events have been observed for the  $\Sigma^-p$  elastic scattering from  $1.62 \times 10^7$   $\Sigma^-$  particles.

The differential cross section was defined by this equation

$$\frac{d\sigma}{d\Omega} = \frac{\sum_{i_{vtz}} \frac{N_{scat}(i_{vtz}, \cos\theta)}{\epsilon(i_{vtz}, \cos\theta)}}{\rho \cdot N_{Avo} \cdot L \cdot d\Omega}, \quad (1)$$

where  $\rho$ ,  $N_{Avo}$  and  $L$  represent the target density, Avogadro's number and the total flight length of the  $\Sigma^-$  hyperons in the LH<sub>2</sub> target, respectively. The values of the numerator depends on the vertex position of the  $\Sigma^-p$  scattering.  $i_{vtz}$  represents the index of the  $z$  vertex position from  $-150$  mm to  $150$  mm with an interval of  $30$  mm.  $N_{scat}(i_{vtz}, \cos\theta)$  and  $\epsilon(i_{vtz}, \cos\theta)$  represent the number of the  $\Sigma^-p$  elastic scattering events and the detection efficiency of CATCH for scattering angle  $\theta$  in the c.m. frame for the  $z$  vertex position of  $i_{vtz}$ , respectively. The total flight length ( $L$ ) could be obtained from a Monte Carlo simulation considering the  $\Sigma^-$  lifetime by using the obtained momentum and vertex information of  $\Sigma^-$  from the spectrometer analysis as inputs of this simulation. As shown in FIG. 2 (a), there were the contamination events in the selected  $\Sigma^-$  mass region due to the misidentification of  $K^+$ . This contribution was subtracted by estimating the flight length of the contamination from the  $K^+$  side-band events in the mass spectrum. The detection efficiency for a proton in CATCH depends on the momentum because the energy loss in the materials in the LH<sub>2</sub> target system and the fibers in CFT becomes large for lower momenta. In order to obtain the realistic efficiency, we took  $pp$  scattering data by employing the proton beam from  $450$  MeV/ $c$  to  $850$  MeV/ $c$  in the K1.8 beam line. By identifying the  $pp$  scattering event by detecting one proton, the other proton's angle and momentum can be predicted as the missing momentum of the  $pp \rightarrow pX$  reaction. The CATCH efficiency was obtained by checking whether the predicted track was detected or not. The detector acceptance and the analysis efficiency were obtained from a Monte Carlo simulation using the Geant4 package [34] taking into account the realistic detector resolutions. The detection efficiency for the  $\Sigma^-p$  scattering events ( $\epsilon(i_{vtz}, \cos\theta)$ ) was obtained based on the CATCH efficiency, the detector acceptance and the analysis efficiency. Differential cross sections of the  $np$  scattering were also derived from the peak counts in the  $\Delta E(np)$  spectra to check the validity of derived efficiency and these values were consistent with past data within  $3\sigma$ .

Figure 4 shows the measured differential cross sections with a past measurement (KEK-PS E289 data for  $400 < p$  (MeV/ $c$ )  $< 700$  [21]) and theoretical calculations.

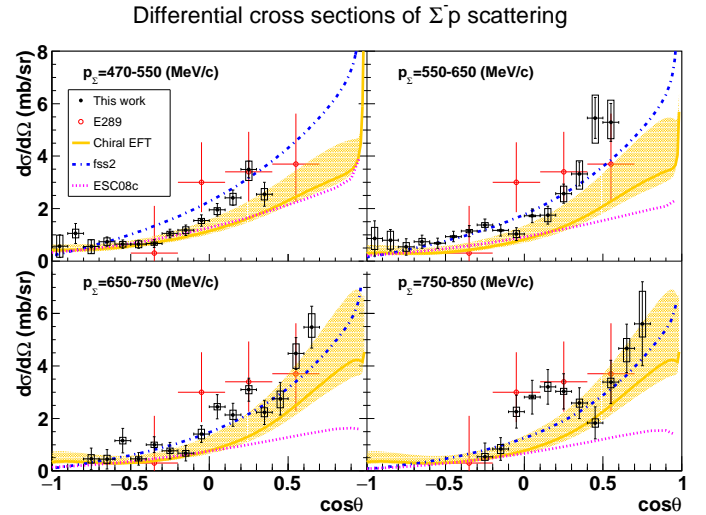


FIG. 4. Differential cross sections obtained in the present experiment (black points). The error bars and boxes show statistical and systematic uncertainties, respectively. Red points are averaged differential cross section of  $400 < p$  (MeV/ $c$ )  $< 700$  taken in KEK-PS E289 (the same points are plotted in all of the four momentum regions). The dotted (magenta), dot-dashed (blue) and solid (yellow) lines represent the calculated cross sections by the Nijmegen ESC08c model based on boson-exchange picture, the fss2 model including QCM and the extended  $\chi$ EFT model, respectively.

Here, the error bars and the black boxes show the statistical and systematic uncertainties, respectively. The systematic uncertainty was estimated as a quadratic sum of systematic error sources whose main components were the uncertainties of the background estimation in the  $\Delta E(\Sigma^-p)$  spectra and the CATCH efficiency. Although the total error becomes large at the edge of the angular acceptance, the data quality has been drastically improved compared with the past experiments. The data show a clear forward-peaking angular dependence for every momentum region, although the statistical fluctuation becomes larger in the momentum higher than  $650$  MeV/ $c$ . Theoretical calculations for each momentum region are also overlaid. The dotted (magenta), dot-dashed (blue) and solid (yellow) lines represent calculations by the Nijmegen ESC08c model based on boson-exchange picture, by the fss2 model which includes QCM and by the extended  $\chi$ EFT, respectively. For every momentum region, the theoretical prediction by fss2 shows a rather good agreement with our data in the angular dependence and its absolute values, although there is a sizable difference at the lower momentum region. The Nijmegen ESC08c model underestimates the differential cross sections at the forward angle. For the  $\chi$ EFT including the error band due to the cut-off value, the calculation with the most reasonable cut-off value also underestimates the differential cross section especially in the lower momentum regions. In the present model, the low-energy con-

stants (LEC) representing the short-range part of the interaction were not well fixed due to insufficient experimental data particularly for the high momentum ( $> 300$  MeV/ $c$ ) region. Our data will be an essential input to fix the LEC parameters in the extended  $\chi$ EFT model.

In summary, we successfully measured the differential cross sections of the  $\Sigma^-p$  elastic scattering for the momentum region from 470 to 850 MeV/ $c$  at J-PARC. The statistical error of 10% level was achieved with a fine angular step of  $d\cos\theta = 0.1$  by identifying the largest statistics of about 4,500  $\Sigma^-p$  elastic scattering events from  $1.72 \times 10^7$   $\Sigma^-$  particles. The differential cross sections show clear forward peaking structure and the forward and backward ratio is large particularly in the higher momentum regions. Although the experimental inputs of the two-body hyperon-proton scattering were quite limited up to now, the success of the  $\Sigma^-p$  scattering is a remarkable step to provide accurate data to improve the  $BB$  interaction models and to establish the realistic  $BB$  interactions with both theoretical and experimental efforts. Analysis to derive the differential cross sections of the  $\Sigma^-p \rightarrow \Lambda n$  reaction and the  $\Sigma^+p$  elastic scattering is on going. Because all channels are related to each other within the flavor SU(3) symmetry, these data also impose important constraint on the two-body  $BB$  interaction theories. By synthesizing all the experimental information, better understanding of the  $BB$  interactions will be achieved in near future.

We would like to thank the staffs of the J-PARC accelerator and the Hadron Experimental Facility for their support to provide beam during the beam time. We would also thank the staffs of CYRIC and ELPH at Tohoku University for their support to provide beam for the test experiment for our detectors. We would like to express thanks to Y. Fujiwara for the theoretical support from an early period of the experimental design and thank T. A. Rijken and J. Haidenbauer for their theoretical calculations. We also thank KEKCC and SINET4. This work was supported by JSPS KAKENHI Grant Number 23684011, 15H00838, 15H05442, 15H02079 and 18H03693. This work was also supported by Grants-in-Aid Number 24105003 and 18H05403 for Scientific Research from the Ministry of Education, Culture, Science and Technology (MEXT) Japan.

- 
- [1] T. A. Rijken, V. G. J. Stoks, and Y. Yamamoto, Phys. Rev. C **59**, 21 (1999).
  - [2] M. M. Nagels, T. A. Rijken, and Y. Yamamoto, Phys. Rev. C **99**, 044003 (2019).
  - [3] J. Haidenbauer and U.-G. Meißner, Phys. Rev. C **72**, 044005 (2005).
  - [4] M. Oka, K. Shimizu, and K. Yazaki, Nucl. Phys. A **464**, 700 (1987).
  - [5] Y. Fujiwara, Y. Suzuki, and C. Nakamoto, Prog. Part. Nucl. Phys. **58**, 439 (2007).
  - [6] S. Aoki *et al.*, Prog. Theor. Exp. Phys. , 01A105 (2012).
  - [7] T. Inoue *et al.*, Nucl. Phys. A **881**, 28 (2012).
  - [8] H. Nemura *et al.*, EPJ Web of Conf. **175**, 05030 (2018).
  - [9] J. Haidenbauer, S. Petschauer, N. Kaiser, U.-G. Meißner, A. Nogga, and W. Weise, Nucl. Phys. A **915**, 24 (2013).
  - [10] J. Haidenbauer, U.-G. Meißner, and A. Nogga, Eur. Phys. J. A **56**, 91 (2020).
  - [11] R. Machleidt, Phys. Rev. C **63**, 024001 (2001).
  - [12] V. Stoks, R. Klomp, C. Terheggen, and J. de Swart, Phys. Rev. C **49**, 2950 (1994).
  - [13] R. Wiringa, V. Stoks, and R. Schiavilla, Phys. Rev. C **51**, 38 (1995).
  - [14] B. Sechi-Zorn, B. Kehoe, J. Twitty, and R. A. Burnstein, Phys. Rev. **175**, 1735 (1968).
  - [15] G. Alexander *et al.*, Phys. Rev. **173**, 1452 (1968).
  - [16] J. A. Kadyk, G. Alexander, J. H. Chan, P. Gaposchkin, and G. H. Trilling, Nucl. Phys. B **27**, 13 (1971).
  - [17] J. M. Hauptman, J. A. Kadyk, and G. H. Trilling, Nucl. Phys. B **125**, 29 (1977).
  - [18] R. Engelmann, H. Filthuth, V. Hepp, and E. Kluge, Phys. Lett. **21**, 587 (1966).
  - [19] F. Eisele, H. Filthuth, W. Fölisch, V. Hepp, and G. Zech, Phys. Lett. **37B**, 204 (1971).
  - [20] D. Stephen, Ph.D. thesis (1970).
  - [21] Y. Kondo *et al.*, Nucl. Phys. A **676**, 371 (2000).
  - [22] J. K. Ahn *et al.*, Nucl. Phys. A **761**, 41 (2005).
  - [23] O. Hashimoto and H. Tamura, Prog. Part. Nucl. Phys. **57**, 564 (2006).
  - [24] Y. Yamamoto, T. Motoba, and T. Rijken, Prog. Theor. Phys. Suppl. **185**, 72 (2010).
  - [25] P. Demorest *et al.*, Nature **467**, 1081 (2010).
  - [26] Y. Yamamoto, T. Furumoto, N. Yasutake, and T. A. Rijken, Phys. Rev. C **90**, 045805 (2014).
  - [27] T. Nagae *et al.*, Phys. Rev. Lett. **80**, 1605 (1998).
  - [28] P. Saha *et al.*, Phys. Rev. C **70**, 044613 (2004).
  - [29] T. Harada, R. Honda, and Y. Hirabayashi, Phys. Rev. C **97**, 024601 (2018).
  - [30] K. Miwa *et al.*, AIP Conf. Proc. **2130**, 020006 (2019).
  - [31] K. Miwa *et al.*, J. Phys. : Conf. Ser. **1643**, 012174 (2020).
  - [32] T. Takahashi *et al.*, PTEP **2012**, 02B010 (2012).
  - [33] Y. Akazawa *et al.*, JPS Conf. Proc. **27**, 011008 (2019).
  - [34] S. Agostinelli *et al.*, Nucl. Instrum. Methods Phys. Res., Sect. A **506**, 250 (2003).